Expanding lone pair $\cdots\pi$ interactions to nonaromatic systems and nitrogen bases : complexes of C_2F_3X(X = F, Cl, Br, I) and TMA($-d_9$)

Expanding Lone Pair···π Interactions to Nonaromatic Systems and Nitrogen Bases: Complexes of C_2F_3X (X = F, Cl, Br, I) and TMA(-d_9)

Yannick Geboes[a,b], Frank De Proft[b] and Wouter A. Herrebout[a]*

[a] *Department of Chemistry, University of Antwerp, Groenenborgerlaan 171, 2020 Antwerp (Belgium), E-mail: Wouter.herrebout@uantwerpen.be*
[b] *Eenheid Algemene Chemie (ALGC), Member of the QCMM VUB-UGent Alliance Research Group, Vrije Universiteit Brussel (VUB), Pleinlaan 2, 1050 Brussels (Belgium)*

Abstract

The molecular electrostatic potential surface of unsaturated, locally electron deficient molecules shows a positive region perpendicular to (a part of) the molecular framework. In recent years it has been shown both theoretically and experimentally that molecules are able to form noncovalent interactions with Lewis bases through this π-hole. When studying unsaturated perfluorohalogenated molecules containing a higher halogen atom, a second electropositive region is also observed near the halogen atom. This region, often denoted as a σ-hole, allows the molecules to interact with Lewis bases and form a halogen bond.

To experimentally characterize the competition between both these noncovalent interactions, Fourier transform infrared and Raman spectra of liquefied noble gas solutions containing perfluorohalogenated ethylene derivatives (C_2F_3X; X= F, Cl, Br or I) and trimethylamine(-d_9) were investigated. Analysis of the spectra shows that in mixed solutions of trimethylamine(-d_9) and C_2F_4 or C_2F_3Cl lone pair···π complex is present, while evidence for halogen bonded complex is found in solutions containing TMA(-d_9) and C_2F_3Cl, C_2F_3Br or C_2F_3I. For all species observed, complexation enthalpies were determined, the values varying between -4.9(1) and -24.4 kJ mol^{-1}.

Keywords: FTIR, Raman, Noncovalent, Lone Pair···π, Halogen Bonding

1. Introduction

Halogen bonds (XB) have gained a large increase in interest during the past decade in the fields of supramolecular chemistry and crystal engineering[1] as well as biochemistry, molecular recognition and rational drug design.[2-3] Thanks to this increased interest, halogen bonds have now been studied extensively both theoretically and experimentally.

The existence of halogen bonding has been characterized theoretically by the presence of a positive region in the electrostatic potential surface near the halogen atom, opposite to the covalent bond, the so-called σ-hole.[4] Since the strength of halogen bonds strongly depends on both the involved halogen

atom and the properties of the molecule to which it is covalently bonded, it is possible to tune the strength of the noncovalent interaction by altering the halogen atom or the properties of the covalently bonded molecule.[5-6] In many applications relatively strong interactions are preferred, which has, especially in the field of supramolecular chemistry, led to the use of molecules containing strong electron withdrawing moieties, such as highly halogenated, or more specifically highly fluorinated, molecules as halogen bond donors. Thanks to the work of Resnati and Metrangolo, perfluorohalocarbons (PFHC's) are nowadays considered "iconic" halogen bond donors.[7-8]

However, when the locally strongly electron deficient molecules are also unsaturated, they can exhibit a region of positive electrostatic potential perpendicular to the molecular plane. In analogy with the term σ-hole, such a positive region, perpendicular to a portion of the molecular framework, is called a π-hole.[9] To illustrate this π-hole, as well as the σ-hole, the electrostatic potential surfaces of C_2F_4, C_2F_3Cl, C_2F_3Br and C_2F_3I are shown in Figure 1.

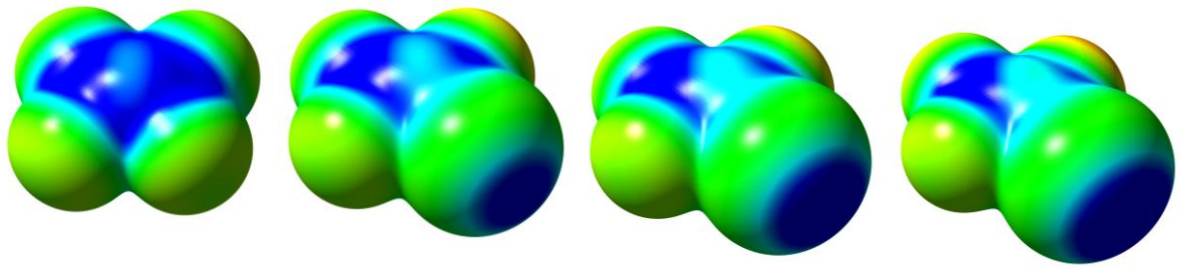

Figure 1: Electrostatic potential of C_2F_4 (left), C_2F_3Cl, C_2F_3Br and C_2F_3I (right) on the molecular surface defined by the 0.001 electrons $Bohr^{-3}$ contour of the electron density, with positive, neutral and negative regions shown in blue, green and red, respectively.

In recent years, attractive noncovalent interactions between these regions of positive electrostatic potential and electron rich sites in Lewis bases, often called lone pair-π interactions (lp···π), have also been observed in theoretical[10-12] and experimental studies.[13-18] These studies have demonstrated that lp···π interactions occur most commonly through oxygen,[19-20] largely because of the overwhelming biological importance of water.[13-14] Theoretical and experimental information on lp···π interactions involving other electron donors, such as nitrogen, still remains scarce.[21-24]

Furthermore, in nearly all of these studies the π-system in the bond donor molecule is based on an aromatic ring structure.[25] The effect of electron withdrawing groups leading to electron deficiency in the π system, is however not restricted to aromatic compounds. In a previous study published by our group, we have demonstrated the lp···π bonding possibility of a non-aromatic system of the C_2F_3X (X=F, Cl, Br, I) type with the oxygen lone pair of dimethyl ether (DME).[26] The choice for DME was based on the biochemical significance of the oxygen···π interaction with the water molecule, as well as the limitations of the used experimental equipment and techniques, which don't allow for the straightforward analysis of complexes involving strong self-associating molecules such as water.

The aim of this study is to build further on the findings of Gou et al.,[27] in which the existence of the lp···π complex of $C_2F_3Cl{\cdot}NH_3$ was demonstrated using pulsed-jet Fourier transform microwave spectroscopy, and expand the field of lp···π interactions at thermodynamic equilibrium to systems with a non-aromatic bond donor and the lone pair of a nitrogen atom. This is achieved by experimentally studying mixtures of a trifluorohaloethylene-moiety C_2F_3X (X= F, Cl , Br or I), which has an electron deficient π-system, with the Lewis base trimethylamine (TMA) in noble gas solutions using Fourier transform infrared (FTIR) and Raman spectroscopy. In order to avoid spectral congestion and aid assignment of the complex bands, measurements are performed using regular TMA and fully deuterated TMA-d_9. When referring to (measurements or results of) both undeuterated and fully deuterated TMA the notation TMA(-d_9) is used in the remainder of this paper. The final aim of this study is to investigate whether lp···π interactions involving the lp of a nitrogen atom can be observed in an environment at thermodynamic equilibrium and if they are able to coexist and/or compete with competitive halogen bonds under these conditions.

2. Experimental

The samples of tetrafluoroethylene (C_2F_4, 99%) bromotrifluoroethylene (C_2F_3Br, 98%) and chlorotrifluoroethylene (C_2F_3Cl, 99%) were purchased from ABCR. Iodotrifluoroethylene (C_2F_3I, 97%) was obtained from Lancaster while the samples of trimethylamine (TMA, 99%) and fully deuterated trimethylamine (TMA-d_9, 99 atom% D) were purchased from Sigma-Aldrich. The solvent gas krypton was supplied by Air Liquide and had a stated purity of 99.9995%. Xenon was supplied by Linde and had a stated purity of 99.999%. All products were used without further purification.

The infrared spectra were recorded on a Bruker 66v FTIR spectrometer, equipped with a globar source, a Ge/KBr beam splitter and MCT detector, cooled with liquid nitrogen. All interferograms were averaged over 500 scans, Blackman-Harris 3-term apodized and Fourier transformed with a zero filling factor of 8 to yield spectra with a resolution of 0.5 cm^{-1}. Thermal expansion of the solvent gas during temperature studies was accounted for using the method published by van der Veken.[28]

Raman spectra were recorded using a Trivista 557 spectrometer consisting of a double f = 50 cm monochromator equipped with 300/1500/2000 lines mm^{-1} gratings and a f = 70 cm spectrograph equipped with 500/1800/2400 lines mm^{-1} gratings and a back-end illuminated LN_2 cooled CCD detector. The 514.5 nm line of a Spectra-Physics Stabilite 2017 argon ion laser was used for Raman excitation, the power of the incident laser beam was set to 0.8 W. Frequencies were calibrated using Ne emission lines, and are expected to be accurate to 0.5 cm^{-1}.

To support our experimental measurements, *ab initio* MP2 calculations were performed using Dunning's augmented correlation consistent basis sets of double (aug-cc-pVDZ) or triple (aug-cc-pVTZ) zeta quality in Gaussian09.[29] The standard aug-cc-pVDZ and aug-cc-pVTZ basis sets were used for hydrogen, carbon, nitrogen, fluorine and chlorine, while aug-cc-pVDZ-PP and aug-cc-pVTZ-PP basis sets including small-core energy-consistent relativistic pseudopotentials (PP) were used for bromine and iodine.[30-31] The counterpoise technique as proposed by Boys and Bernardi was used during all *ab initio* calculations to account for basis set superposition error.[32] Energies at the basis set limit were calculated with Molpro[33] using the extrapolation scheme of Truhlar, in which the effect of electron correlation is obtained from MP2 calculations.[34]

$$E_{CBS}^{HF} = \frac{3^{\alpha}}{3^{\alpha} - 2^{\alpha}} E_3^{HF} - \frac{2^{\alpha}}{3^{\alpha} - 2^{\alpha}} E_2^{HF} \quad (1)$$

$$E_{CBS}^{cor,MP2} = \frac{3^{\beta}}{3^{\beta} - 2^{\beta}} E_3^{cor,MP2} - \frac{2^{\beta}}{3^{\beta} - 2^{\beta}} E_2^{cor,MP2} \quad (2)$$

In these calculations α = 3.4 and β=2.2,[34] while energies with subscript 2 and 3 are calculated using the aug-cc-pVDZ(-PP) and aug-cc-pVTZ(-PP) basis sets respectively.

Furthermore, a correction for higher order correlation effects is made using Hobza's method,[35] yielding results of $E_{CBS}^{CCSD(T)}$ quality.

$$\Delta E^{CCSD(T)} = \left| E^{CCSD(T)} - E^{MP2} \right|_{aug-cc-pVDZ(-PP)} \quad (3)$$

$$E_{CBS}^{CCSD(T)} = E_{CBS}^{HF} + E_{CBS}^{cor,MP2} + \Delta E^{CCSD(T)} \quad (4)$$

Complexation enthalpies in the vapor phase ΔH°(vap,calc) were obtained from the calculated complexation energies ΔE(CCSD(T)) by applying a zero-point energy correction and a correction for thermal effects. Correction of these calculated enthalpy values with solvent effects yields complexation enthalpies in solution ΔH°(LNg,calc) which can be compared with the experimental complexation enthalpies ΔH°(LNg). Corrections for thermal effects and zero-point vibrational contributions were obtained using statistical thermodynamics, whereas the effects of solvation were accounted for using the Monte Carlo Free Energy Perturbation (MC-FEP) approach in an in-house modified version of BOSS 4.0.[36]

3. Results

Geometries of both types of complexes with their respective angles are shown in Figure 2. Intermolecular bonding distances and angles as well as calculated energetics for all calculated C_2F_3X·TMA complex geometries have been summarized in Table 1. Cartesian coordinates of all monomers and complex geometries are given in Tables S1 to S12 of the ESI. To enable comparison with halogen bonded complexes formed through C(sp^3) bonded halogen atoms, theoretical results using an identical computational method and experimental results[37] for the equivalent CF_3X·TMA

(X=Cl, Br, I) halogen bonded complexes have also been included in these tables. Explanation of the intermolecular properties is given in Figure S1 of the ESI. As in our previous publication on the C_2F_3X·DME complexes, no stationary point could be found for a halogen bonded geometry between C_2F_4 and TMA, which is consistent with the lack of σ-hole in the electrostatic potential surface in the vicinity of the fluorine atom.[26]

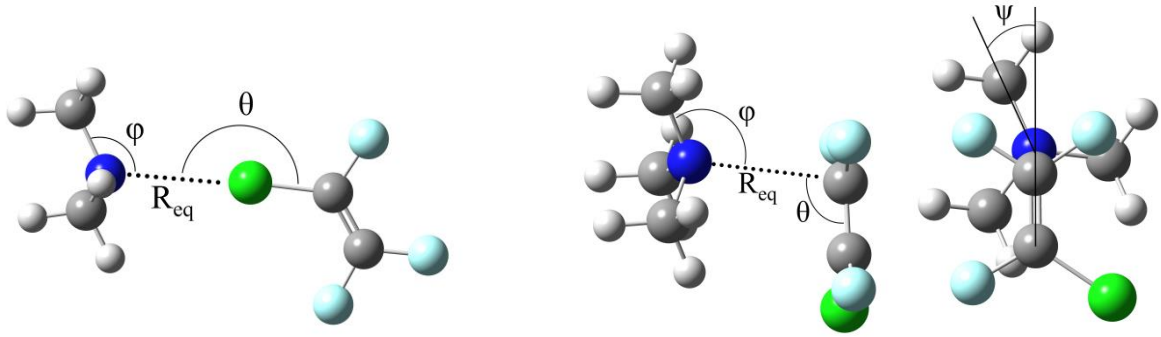

Figure 2: MP2/aug-cc-pVDZ(-PP) equilibrium geometries for the halogen (left) and N···π (right) bonded complexes of C_2F_3X (X = F, Cl, Br and I) with trimethylamine, including the designation of the angles given in Table 1.

Table 1: Intermolecular distance R_{eq} (Å), bond angles and dihedrals (°) and the MP2/aug-cc-pVDZ(-PP) ΔE(DZ), MP2/aug-cc-pVTZ(-PP) ΔE(TZ) and CCSD(T)/CBS ΔE(CCSD(T)) complexation energies (kJ mol^{-1}) for the complexes of C_2F_3X (X = F, Cl, Br, I) with trimethylamine. For completeness, the corresponding values for the complexes of CF_3X (X = Cl, Br, I) with trimethylamine are also given.

N···π bonded	C_2F_4·TMA	C_2F_3Cl·TMA	C_2F_3Br·TMA	C_2F_3I·TMA
$R_{eq}=R_{C=C\cdots N}$	2.95	2.92	2.92	2.92
$\theta_{C=C\cdots N}$	102.2	100.3	100.4	100.9
$\varphi_{C\cdots N-C}$	116.9	117.6	116.9	115.3
$\psi_{C=C\cdots N-C}$	180.0	155.3	152.1	150.2
ΔE (DZ)	-15.1	-18.1	-18.5	-19.1
ΔE (TZ)	-16.5	-19.9	-20.6	-21.4
ΔE (CCSD(T))	-16.8	-19.6	-20.1	-20.6
Halogen bonded	C_2F_3Cl·TMA	C_2F_3Br·TMA	C_2F_3I·TMA	
$R_{eq}=R_{X\cdots N}$	2.98	2.85	2.84	
$\theta_{C-X\cdots N}$	176.4	179.0	178.9	
$\varphi_{C-N\cdots X}$	118.4	108.4	108.4	
ΔE (DZ)	-14.7	-24.6	-36.3	
ΔE (TZ)	-15.3	-25.0	-36.6	
ΔE (CCSD(T))	-15.1	-24.8	-36.0	
Halogen bonded	CF_3Cl·TMA	CF_3Br·TMA	CF_3I·TMA	
$R_{eq}=R_{X\cdots N}$	2.96	2.83	2.82	
$\theta_{C-X\cdots N}$	180.0	180.0	180.0	
$\psi_{F-C\cdots N-C}$	58.3	0.1	0.0	

ΔE (DZ)	-15.2	-25.0	-37.1
ΔE (TZ)	-15.8	-25.3	-37.3
ΔE (CCSD(T))	-15.6	-25.0	-36.5

For the C_2F_3X (X = Cl, Br, I) halogen bonded complexes a strong increase in bonding energy is observed from –15.1 kJ mol^{-1} to -36.0 kJ mol^{-1} at the CCSD(T)/CBS level going from chlorine to iodine, combined with a decrease in bond distance from 2.98 Å to 2.84 Å. For all halogen bonded complexes a nearly linear C-X···N bonding geometry is observed, the bonding angles lying between 176.4 and 179.0°. From Table 1 it is also clear to see that the complexation energy for the lp···π bonded complexes of C_2F_3Cl, C_2F_3Br and C_2F_3I is quite similar, the values lying between -19.6 kJ mol^{-1} and -20.6 kJ mol^{-1} at the CCSD(T)/CBS level, with a slight increase towards the complexes involving donors with a more polarizable halogen atom. For the lp···π bonded complex with C_2F_4, the lower value of –16.8 kJ mol^{-1} can be explained by the lack of secondary C-H···F interactions, whereas secondary C-H···X (X = Cl, Br, I) interactions are present in the other lp···π complexes (*vide infra*). In order to visualize these secondary interactions, the lp···π complexes were analyzed using the noncovalent interactions index visualized using NCIPLOT[38-39], for which the results are given in Figure S2 of the ESI. These images show that apart from the intermolecular interaction surface caused by the lp···π interaction, two additional intermolecular interaction surfaces appear between the hydrogens of TMA and the higher halogen atoms of C_2F_3Cl, C_2F_3Br and C_2F_3I, corresponding to these secondary C-H···X (X = Cl, Br, I) interactions. As mentioned in the previous study of C_2F_3X·DME, the existence of secondary interaction also influences the geometry of the formed lp···π complex. Here, a deviation from the linear C=C···N-C torsion angle ψ of the complex with C_2F_4 is observed for the other three lp···π bonded complexes, with the torsion angle decreasing from 155.3° to 150.2° going from the chlorine to the iodine substituted donor molecule. From the $\theta_{C=C\cdots N}$ angle, which lies between 100.3° and 102.2°, it is also clear that the nitrogen atom does not lie directly above the C(sp^2) atom, but slightly further along the C=C axis, which corresponds to the position of the π* orbital.

An overview of the calculated CCSD(T)/CBS complexation energies and calculated complex enthalpies in the vapor phase and in solution is given in Table 2.

Table 2: Values of the CCSD(T)/CBS complexation energies, the calculated vapor phase complexation enthalpies, the calculated complexation enthalpies in liquid krypton (LKr) or liquid xenon (LXe) and the corresponding experimentally obtained complexation enthalpies for the complexes of C_2F_3X (X = F, Cl, Br, I) with TMA in kJ mol^{-1}. For completeness, the corresponding values for the halogen bonded complexes of CF_3X (X = Cl, Br, I) with TMA, determined in liquid argon (LAr), LKr or LXe are also given.

	N···π interaction				halogen bond			halogen bond		
	C_2F_4	C_2F_3Cl	C_2F_3Br	C_2F_3I	C_2F_3Cl	C_2F_3Br	C_2F_3I	CF_3Cl	CF_3Br	CF_3I
Δ*E* (CCSD(T))	-16.8	-19.6	-20.1	-20.6	-15.1	-24.8	-36.0	-15.6	-25.0	-36.5
Δ*H*° (vap,calc)	-14.5	-17.2	-17.7	-17.3	-12.7	-22.2	-32.1	-13.7	-22.4	-32.6

Δ*H*° (LXe,calc)				-9.2			-31.6					-32.2
Δ*H*° (LKr,calc)	-7.8	-9.3	-9.5		-9.5	-19.7				-19.9		
Δ*H*° (LAr,calc)								-10.2				
Experimental												
Δ*H*° (LXe)							-24.4(2)					-28.7(1)
Δ*H*° (LKr)	-4.9(2)	-4.9(1)			-8.3(4)	-15.7(3)				-18.3(1)		
Δ*H*° (LAr)								-8.9(2)				

In order to distinguish the different complex geometries, vibrational modes in which both isomers have sufficiently different calculated complexation shifts, preferably one redshifted and the other blueshifted, have been selected for further experimental study. By analyzing the *ab initio* calculated shifts, given in Tables S13 to S26 of the ESI, three modes of interest were selected for further experimental study. The numbering of the fundamental vibrational modes of all compounds follows the numbering scheme of Herzberg.[40]

The first mode concerns the C=C stretching vibration, which for all four C_2F_3X (X = F, Cl, Br, I) compounds has a calculated blueshift for the lp···π complex and a redshift for the XB complex. The observation that the lp···π interactions cause a blueshift for the C=C stretching mode contradicts with the general expectation[41] that these types of complexes are characterized by a charge transfer from the lone pair to the π* orbital and thus should be characterized by a weakening of the C=C bond. To shed more light on the underlying nature of this contradiction, an NBO analysis of the lp···π interaction was attempted. Unfortunately, due to many different energetic contributions to the interaction energy, this analysis did not offer a clear indication whether the interaction can be ascribed solely to a pure n→π* interaction.

The calculated blueshifts for the lp···π complex are 3.2 cm^{-1}, 4.0 cm^{-1}, 4.0 cm^{-1} and 3.9 cm^{-1} for the complexes involving C_2F_4, C_2F_3Cl, C_2F_3Br and C_2F_3I respectively, while the calculated redshifts for the XB complexes of the latter three compounds are -5.3 cm^{-1}, -8.7 cm^{-1} and -12.1 cm^{-1} respectively. It should however also be noted that this vibrational mode has A_g symmetry for C_2F_4, and thus has no IR intensity. Experimental study of this vibrational mode will therefore be conducted using Raman spectroscopy.

IR spectra of the C=C stretching region of the C_2F_3X (X = F, Cl, Br, I) are shown in Figure 3 for the complexes with TMA and in Figure S3 of the ESI for the complexes with TMA-d_9. Raman spectra for the same spectral regions are also given in Figures 4 (TMA) and S4 (TMA-d_9).

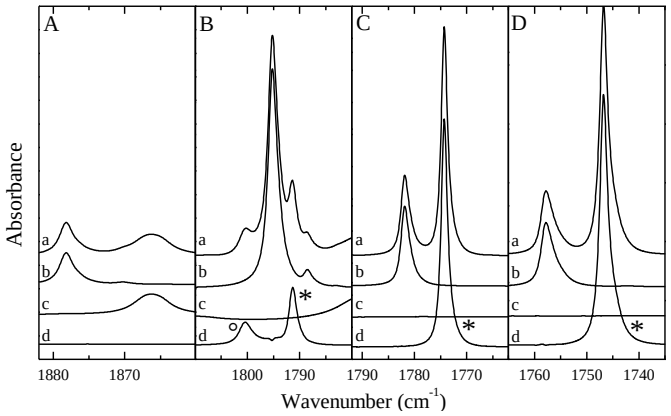

Figure 3: Infrared spectra of the $\nu_{C=C}$ spectral region of C_2F_3X (X = F, Cl, Br, I) for solutions of mixtures of trimethylamine with C_2F_4 (panel A), C_2F_3Cl (panel B), C_2F_3Br (panel C) and C_2F_3I (panel D) dissolved in LKr at 120 K for panels A-C and LXe at 170 K for panel D. In each panel, trace *a* represents the mixed solution, while traces *b* and *c* show the solution containing only C_2F_3X or trimethylamine, respectively. Trace *d* represents the spectrum of the complex and is obtained by subtracting the rescaled traces *b* and *c* from trace *a*. New bands due to the 1:1 C(sp^2)-X···N halogen bonded and the 1:1 lp···π bonded complexes are marked with an asterisk (*) and an open circle (°), respectively.

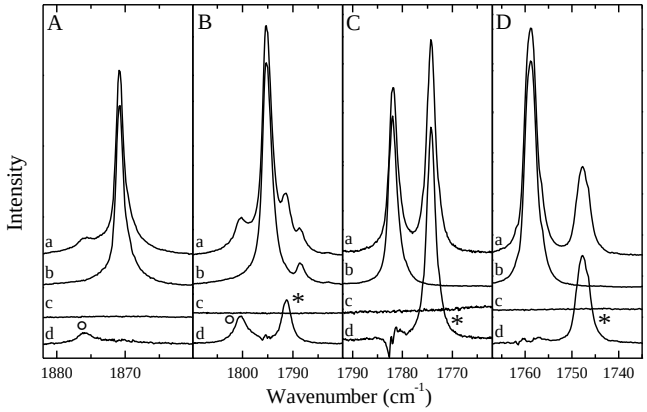

Figure 4: Raman spectra of the $\nu_{C=C}$ spectral region of C_2F_3X (X = F, Cl, Br, I) for solutions of mixtures of trimethylamine with C_2F_4 (panel A), C_2F_3Cl (panel B), C_2F_3Br (panel C) and C_2F_3I (panel D) dissolved in LKr at 120 K. In each panel, trace *a* represents the mixed solution, while traces *b* and *c* show the solution containing only C_2F_3X or trimethylamine, respectively. Trace *d* represents the spectrum of the complex and is obtained by subtracting the rescaled traces *b* and *c* from trace *a*. New bands due to the 1:1 C(sp^2)-X···N halogen bonded and the 1:1 lp···π bonded complexes are marked with an asterisk (*) and an open circle (°), respectively.

In the Raman spectra of C_2F_4·TMA(-d_9), shown in panels 4A and S4A, a weak blueshifted complex band can be observed in the spectra of the mixtures. This band, which is blueshifted by 5.1 cm^{-1}, corresponds well to the calculated shift of 3.2 cm^{-1} for the lp···π complex.

For the mixtures of C_2F_3Cl and TMA(-d_9), shown in panels 3B, 4B, S3B and S4B, two complex bands are observed in the C=C stretching region upon subtraction. The blueshifted band with a complexation shift of 5.2 cm^{-1} can be assigned to the lp···π bonded complex with a calculated shift of 4.0 cm^{-1},

whereas the -3.9 cm^{-1} redshifted band agrees very well with the calculated value of -5.3 cm^{-1} for the halogen bonded complex.

For the mixtures involving C_2F_3Br, shown in panels 3C, 4C, S3C and S4C, only a -7.5 cm^{-1} redshifted band is observed in the C=C stretching region, which agrees well with the calculated value of -8.7 cm^{-1} for the XB complex. No blueshifted band corresponding to the lp···π complex, which has a calculated shift of 4.0 cm^{-1}, is observed in any of the spectra.

Due to the relatively high complexation strength of the C_2F_3I·TMA complex, combined with the necessity to retain a discernible amount of both monomers for the temperature studies, FTIR measurements of this complex were performed in LXe, enabling the use of a higher temperatures.[42]

In the IR (panels 3D and S3D) and Raman (panels 4D and S4D) spectra, a strong complex band is observed with a -11.0 cm^{-1} redshift which is assigned to the XB complex with a calculated shift of -12.1 cm^{-1}. Again, no indications were found for the presence of the lp···π complex for this bond donor.

A second region where both complex geometries can be distinguished based on the frequency calculations is found in the region of the antisymmetric CF_2 stretching mode, shown in Figure 5 for complexes involving TMA and Figure S5 of the ESI for the complexes of TMA-d_9. For this vibrational mode, a redshift of -8.8, -12.8 and -18.0 cm^{-1} is predicted for the halogen bonded complexes with C_2F_3Cl, C_2F_3Br and C_2F_3I respectively, whereas blueshifts of 3.1, 3.4 and 3.7 cm^{-1} are predicted for the equivalent lp···π bonded complexes. For C_2F_4, the *cis* and *trans* C-F stretching vibrations (ν_9 and ν_5 respectively) can be found in this spectral region. However, since the *trans* C-F stretching vibration ν_5 is IR inactive, only the *cis* C-F stretching mode is observed in IR, which has a calculated complexation shift of -10.6 cm^{-1} for the lp···π complex.

Since the vibrational modes in this spectral region have a limited Raman intensity, they were not studied experimentally using Raman spectroscopy.

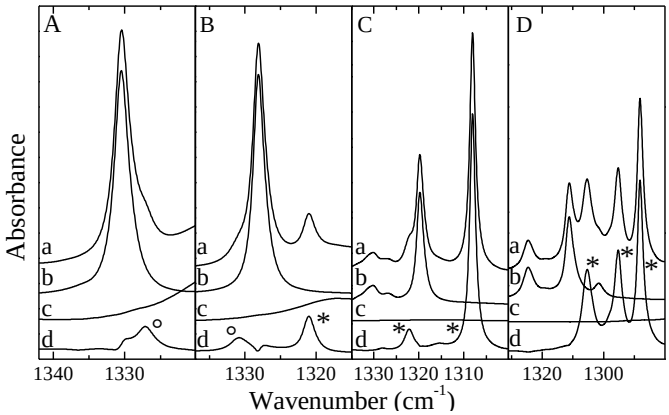

Figure 5: Infrared spectra of the C-F stretching region of C_2F_3X (X = F, Cl, Br, I) for solutions of mixtures of trimethylamine with C_2F_4 (panel A), C_2F_3Cl (panel B), C_2F_3Br (panel C) and C_2F_3I (panel D) dissolved in LKr at 120 K for panels A-C and LXe at 170 K for panel D. In each panel, trace *a* represents the mixed solution, while traces *b* and *c* show the solution containing only C_2F_3X or trimethylamine, respectively. Trace *d* represents the spectrum of the complex and is obtained by

subtracting the rescaled traces *b* and *c* from trace *a*. New bands due to the 1:1 C(sp^2)-X···N halogen bonded and the 1:1 lp···π bonded complexes are marked with an asterisk (*) and an open circle (°), respectively.

For C_2F_4, spectra of the *cis* C-F stretching region (ν_9) are shown in panels 5A and S5A. For this transition, a complex band with a redshift of -3.4 cm^{-1} is isolated using the subtraction method, which is assigned to the lp···π complex with a calculated redshift of -10.6 cm^{-1}.

For the ν_2 antisymmetric CF_2 stretching mode of C_2F_3Cl, shown in panels 5B and S5B, two complex bands with shifts of -7.1 cm^{-1} and 2.7 cm^{-1} are observed, which are assigned to the XB complex with a calculated shift of -8.8 cm^{-1} and the lp···π complex with a calculated complexation shift of 3.5 cm^{-1} respectively.

For the mixtures involving TMA and C_2F_3I or C_2F_3Br, shown in panels 5D and 5C respectively, only redshifted complexation bands are observed, corresponding to the halogen bonded isomers, the calculated and experimental complexation shifts being -18.0 cm^{-1} and -15.9 cm^{-1} for C_2F_3I and -12.8 cm^{-1} and -11.7 cm^{-1} for C_2F_3Br.

Further indication of the coexistence of the lp···π and halogen bonded complex in C_2F_3Cl·TMA($-d_9$) mixtures is found for the ν_{10} vibrational mode, of which the spectral region is shown in Figure 6. Subtraction yields two complex bands with experimental shifts of -0.5 and -2.0 cm^{-1} , corresponding to the halogen and lp···π bonded complex respectively, which have calculated shifts of -1.4 and -9.1 cm^{-1}.

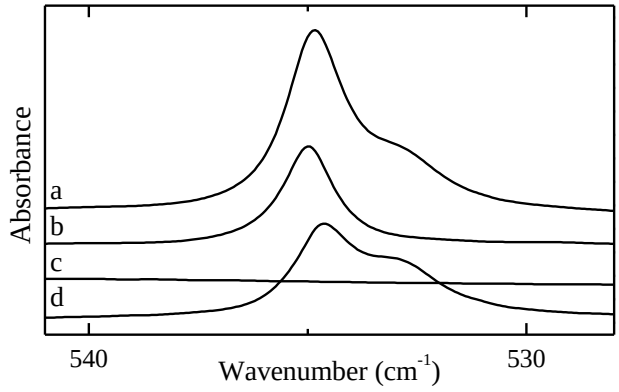

Figure 6: Infrared spectra of the ν_{10} vibrational mode of a C_2F_3Cl mixtures with trimethylamine, dissolved in LKr at 120 K. Trace *a* represents the mixed solution, while traces *b* and *c* show the solution containing only C_2F_3Cl or trimethylamine, respectively. Trace *d* represents the spectrum of the complex and is obtained by subtracting the rescaled traces *b* and *c* from trace *a*. New bands due to the 1:1 C(sp^2)-X···N halogen bonded and the 1:1 lp···π bonded complexes are marked with an asterisk (*) and an open circle (°), respectively.

A full overview of the assignment of the vibrational modes for all monomers and complexes is given in Tables 3 to 6 for the complexes involving TMA and Tables S27 to S30 for the complexes involving TMA-d_9.

Table 3: Experimental vibrational frequencies for the monomer and complexes, as well as experimental complexation shifts ($\Delta\nu_{exp}$) and MP2/aug-cc-pVDZ calculated complexation shifts ($\Delta\nu_{calc,\ N\cdots\pi}$), in cm^{-1}, for the N···π bonded complex (N···π) of C_2F_4 with TMA dissolved in LKr at 120 K.

	Assignment	$\nu_{monomer}$	$\nu_{complex}$	$\Delta\nu_{exp}$	$\Delta\nu_{calc,N\cdots\pi}$
C_2F_4	$\nu_1+\nu_9$	3196.6	3196.6	0.0	-7.5
	$\nu_1+\nu_{11}$	3045.3	3048.4	3.1	-1.0
	ν_1	1870.8	1875.9	5.1	3.2
	ν_9	1330.5	1327.1	-3.4	-10.6
	ν_{11}	1179.5	1177.9	-1.6	-4.1
	ν_2	778.1	777.8	-0.3	-3.3
	ν_{12}	554.7	554.4	-0.3	-0.9
	ν_6	549.9	550.0	0.1	-0.4
	ν_8	505.5	501.0	-4.5	-13.6
	ν_3	395.5	395.4	-0.1	-0.9
TMA	ν_{12}	2977.0	2980.8	2.8	-3.1
	ν_1	2944.4	2947.1	2.7	-0.4
	ν_{13}	2944.4	2947.1	2.7	-3.9
	$2\nu_4$	2818.3	2822.0	3.7	1.7
	ν_2	2768.6	2778.7	10.1	6.9
	ν_{14}	2768.6	2778.7	10.1	7.6
	$\nu_{20}+\nu_{21}$	1474.8	1472.7	-2.1	0.9
	ν_{15}	1467.6	1470.1	2.5	0.7
	ν_3	1454.8	1454.5	-0.3	-0.8
	ν_4	1438.8	1440.6	1.8	0.8
	ν_{16}	1438.8	1440.6	1.8	-1.1
	ν_5	1184.3	[a]		2.3
	ν_{19}	1098.5	1099.0	0.5	-1.2
	ν_{20}	1041.4	1040.0	-1.4	-0.2
	ν_6	828.1	826.1	-2.0	-2.0

[a] Band could not be isolated due to overlap with C_2F_4 modes.

Table 4 : Experimental vibrational frequencies for the monomer and complexes, as well as experimental complexation shifts ($\Delta\nu_{exp}$) and MP2/aug-cc-pVDZ calculated complexation shifts ($\Delta\nu_{calc}$), in cm^{-1}, for the halogen bonded complex (HalB) and N···π bonded complex (N···π) of C_2F_3Cl with TMA dissolved in LKr at 120 K.

			HalB			N···π		
	Assignment	$\nu_{monomer}$	$\nu_{complex}$	$\Delta\nu_{exp}$	$\Delta\nu_{calc}$	$\nu_{complex}$	$\Delta\nu_{exp}$	$\Delta\nu_{calc}$
C_2F_3Cl	ν_1	1795.2	1791.3	-3.9	-5.3	1800.4	5.2	4.0
	ν_1 (^{13}C)	1788.5	[a]		-5.3	[a]		4.0
	ν_2	1328.1	1321.0	-7.1	-8.8	1330.8	2.7	3.1
	ν_3	1214.3	1210.6	-3.7	-8.1	1210.6	-3.7	-7.9
	$2\nu_{10}$	1074.8	1073.1	-1.7		1073.1	-1.7	
	ν_4	1053.7	[b]		-3.9	1052.6	-1.1	-1.9
	ν_5 (^{35}Cl)	691.2	689.3	-1.9	-4.7	691.0	-0.2	-2.1
	ν_5 (^{37}Cl)	689.6	687.6	-2.0	-4.7	689.3	-0.3	-2.1
	ν_{10}	535.0	534.5	-0.5	-1.4	533.0	-2.0	-9.1
	ν_6	516.3	516.7	0.4	0.7	516.0	-0.3	0.1

	ν_7 (^{35}Cl)	462.4	458.3	-4.1	-5.8	462.0	-0.4	-1.0
	ν_7 (^{37}Cl)	456.5	452.4	-4.1	-5.8	456.3	-0.2	-1.0
	ν_8	338.1	340.1	2.0	2.6	[a]		-1.1
	ν_9	189.8	[a]		8.6	[a]		-0.1
TMA	ν_{12}	2977.0	2978.2	1.2	-1.0	2978.2	1.2	-2.6
	ν_1	2944.4	2945.4	1.0	0.4	2945.4	1.0	-0.4
	ν_{13}	2944.4	2945.4	1.0	-0.3	2945.4	1.0	-3.3
	$2\ \nu_4$	2818.6	2822.4	3.8	1.5	2822.4	3.8	0.8
	ν_2	2769.0	2772.6	3.6	8.5	2772.6	3.6	7.1
	ν_{14}	2769.0	2772.6	3.6	9.6	2772.6	3.6	7.8
	$\nu_{20}+\nu_{21}$	1474.8	1473.8	-1.0	-1.8	1473.8	-1.0	-1.8
	ν_{15}	1467.6	1468.1	0.5	0.4	1468.1	0.5	0.5
	ν_3	1454.8	1454.6	-0.2	-0.4	1454.6	-0.2	-1.1
	ν_4	1438.8	1439.3	0.5	0.8	1439.3	0.5	0.4
	ν_{16}	1438.8	1439.3	0.5	-0.8	1439.3	0.5	-1.5
	ν_{17}	1405.3	1406.3	1.0	0.5	1406.3	1.0	0.0
	ν_{18}	1273.3	1271.8	-1.5	-0.3	1271.8	-1.5	-0.6
	ν_5	1184.3	1187.7	3.4	3.4	1187.7	3.4	2.7
	ν_{19}	1098.5	1098.7	0.2	-1.0	1098.7	0.2	-1.3
	ν_{20}	1041.5	[b]		-0.7	[b]		-0.7
	ν_6	828.1	827.4	-0.7	-2.1	827.4	-0.7	-2.3
	ν_{21}	424.0	422.4	-1.6	-1.1	422.4	-1.6	-1.1
	ν_7	372.6	380.2	7.6	5.8	380.2	7.6	6.1

[a] Complex band has not been observed.

[b] Bands could not be isolated due to overlap between the C_2F_3Cl ν_4-mode and TMA ν_{20}-mode.

Table 5: Experimental vibrational frequencies, experimental complexation shifts and MP2/aug-cc-pVDZ-PP calculated complexation shifts ($\Delta\nu_{calc,HalB}$), in cm^{-1}, for the halogen bonded complex of C_2F_3Br with TMA dissolved in LKr at 120 K. For completeness, the MP2/aug-cc-pVDZ-PP calculated complexation shifts of the N$\cdots\pi$ bonded complexes ($\Delta\nu_{calc,N\cdots\pi}$) are also given.

	Assignment	$\nu_{monomer}$	$\nu_{complex}$	$\Delta\nu_{exp}$	$\Delta\nu_{calc,HalB}$	$\Delta\nu_{calc,N\cdots\pi}$
C_2F_3Br	ν_1	1781.8	1774.3	-7.5	-8.7	4.0
	ν_2	1319.8	1308.1	-11.7	-12.8	3.4
	ν_3	1197.2	1184.9	-12.3	-12.9	-7.1
	$2\ \nu_{10}$	1072.6	1071.7	-0.9	-0.8	-20.1
	$\nu_5+\nu_7$ (^{79}Br)	1034.4	1024.3	-10.1	-6.2	-1.2
	$\nu_5+\nu_7$ (^{81}Br)	1033.3	1024.3	-9.0	-6.2	-1.2
	$2\nu_6$	1018.8	1018.6	-0.2	0.8	0.2
	ν_4	1016.6	1006.9	-9.7	-6.2	-1.2
	ν_5	663.9	659.3	-4.6	-5.7	-1.4
	ν_{10}	535.2	534.7	-0.5	-0.4	-10.0
	ν_6	509.1	509.7	0.6	0.4	0.1
	ν_7	365.8	352.3	-13.5	-14.6	0.5
	ν_8	311.1	310.8	-0.3	-0.3	-1.0
	ν_9	162.2	168.8	6.6	9.9	0.2
TMA	ν_{12}	2977.0	2980.3	3.3	1.2	-2.7
	ν_1	2944.4	2952.8	8.4	3.1	-0.5
	ν_{13}	2944.4	2952.8	8.4	3.4	-3.4
	$2\ \nu_4$	2818.6	2827.9	9.3	1.3	0.4

ν_2	2769.0	2778.8	9.8	17.9	6.6
ν_{14}	2769.0	2778.8	9.8	19.8	7.3
$\nu_{20}+\nu_{21}$	1474.8	1472.8	-2.0	-4.4	-1.9
ν_{15}	1467.6	1468.3	0.7	0.4	0.3
ν_3	1454.8	1453.5	-1.3	0.2	-1.2
ν_4	1438.8	1440.0	1.2	0.7	0.2
ν_{16}	1438.8	1440.0	1.2	-0.9	-1.6
ν_{18}	1273.3	1270.2	-3.1	-1.3	-0.7
ν_5	1184.3	1192.4	8.1	7.3	2.6
ν_{19}	1098.5	1098.6	0.1	-1.4	-1.3
ν_{20}	1041.5	1037.9	-3.6	-2.6	-0.8
ν_6	828.1	826.2	-1.9	-4.0	-2.3
ν_{21}	424.0	422.1	-1.9	-1.8	-1.1
ν_7	372.6	388.9	16.3	14.7	5.8
ν_{22}	277.9	272.2	-5.7	-6.6	-2.2

Table 6: Experimental vibrational frequencies, experimental complexation shifts and MP2/aug-cc-pVDZ-PP calculated complexation shifts ($\Delta\nu_{calc,HalB}$), in cm^{-1}, for the halogen bonded complex of C_2F_3I with TMA dissolved in LXe at 170 K. For completeness, the MP2/aug-cc-pVDZ-PP calculated complexation shifts of the $N\cdots\pi$ bonded complexes ($\Delta\nu_{calc,N\cdots\pi}$) are also given.

	Assignment	$\nu_{monomer}$	$\nu_{complex}$	$\Delta\nu_{exp}$	$\Delta\nu_{calc,HalB}$	$\Delta\nu_{calc,N\cdots\pi}$
C_2F_3I	ν_1	1757.8	1746.8	-11.0	-12.1	3.9
	ν_1 (^{13}C)	1742.3	1731.5	-10.8	-12.1	3.9
	$\nu_4+\nu_7$	1324.6	1305.4	-19.2	-21.2	-0.2
	ν_2	1311.2	1295.3	-15.9	-18.0	3.7
	$2\nu_5$	1301.6	1288.2	-13.4	-11.9	-2.3
	ν_3	1173.9	1158.7	-15.2	-17.3	-6.5
	$\nu_5+\nu_6$	1155.2	1146.3	-8.9	-5.9	-1.0
	$2\nu_{10}$	1076.4	1075.0	-1.4	-0.7	-20.5
	$2\nu_6$	1012.5	1011.2	-1.3	0.1	0.3
	ν_4	1001.2	995.6	-5.6	-7.2	-0.8
	ν_{10}	537.5	536.6	-0.9	-0.3	-10.2
	ν_6	506.4	505.7	-0.7	0.03	0.1
	ν_7	321.1	307.4	-13.7	-14.0	0.6
	ν_8	286.8	276.7	-10.1	-9.8	-1.0
TMA	ν_{12}	2977.0	2979.9	2.9	5.2	-2.8
	ν_1	2944.4	2951.3	6.9	8.6	-0.5
	ν_{13}	2944.4	2951.3	6.9	9.1	-3.6
	$2\nu_4$	2818.3	2838.7	20.4	0.3	0.1
	ν_2	2768.6	2782.6	14.0	31.0	6.3
	ν_{14}	2768.6	2782.6	14.0	33.9	6.9
	$\nu_{20}+\nu_{21}$	1474.8	1470.2	-4.6	-9.0	-2.1
	ν_{15}	1467.6	1467.1	-0.5	0.2	0.1
	ν_3	1454.8	1450.1	-4.7	1.3	-1.3
	ν_4	1438.8	1440.3	1.5	0.1	0.0
	ν_{16}	1438.8	1440.3	1.5	-0.9	-1.8
	ν_{18}	1273.4	1267.0	-6.4	-4.2	-0.8
	ν_5	1184.3	1196.8	12.5	12.4	2.5
	ν_{19}	1098.5	1097.7	-0.8	-2.0	-1.5
	ν_{20}	1041.4	1033.3	-8.1	-6.3	-0.9

ν_6	828.1	825.5	-2.6	-7.2	-2.4
ν_{21}	424.0	421.4	-2.4	-2.7	-1.2
ν_7	372.6	403.1	30.5	28.0	5.7

After these assignments, complex enthalpies were determined by creating van 't Hoff plots. An illustration of these van 't Hoff plots is given in Figures S6 and S7 of the ESI. For the halogen bonded complexes of C_2F_3I·TMA(-d_9) in LXe and C_2F_3Br·TMA(-d_9) in LKr, average complexation enthalpies of -24.4(2) kJ mol^{-1} and -15.7(3) kJ mol^{-1} respectively were determined. For the complexes of C_2F_3Cl and TMA(-d_9) a complexation enthalpy of -8.3(4) kJ mol^{-1} was found for the halogen bonded complex, whereas the lp···π bonded complex had a complexation enthalpy of -4.9(1) kJ mol^{-1}. For the lp···π bonded complex with C_2F_4 an experimental complexation enthalpy of -4.9(2) kJ mol^{-1} was found. An overview of all experimental complexation enthalpies is given in Table 2.

4. Discussion

Mixtures involving C_2F_4 and TMA(-d_9) yield complex bands which, based on the *ab initio* frequency calculations, can all be assigned to the lp···π bonded complex. Using these complex bands, an experimental complexation enthalpy of -4.9(2) kJ mol^{-1} was determined. Consistent with the lack of σ-hole in the electrostatic potential surface, no halogen bonded (XB) complex is formed in these mixtures.

For the mixtures of C_2F_3Cl and TMA(-d_9), well separated complex bands for both complex isomers are observed for several vibrational modes, thus proving the coexistence of the halogen bonded and lp···π bonded complexes in these solutions. Complexation enthalpies of -8.3(4) kJ mol^{-1} and -4.9(1) kJ mol^{-1} were measured for the XB and lp···π complex respectively.

As opposed to our previous publication involving DME,[26] no indications at all were found for the presence of lp···π bonded complex in the mixtures of C_2F_3Br and TMA. This is in line with the calculated difference in complexation enthalpy of 10.2 kJ mol^{-1} between both complexes at the CCSD(T)/CBS level, as opposed to 3.9 kJ mol^{-1} for the complexes involving DME. For the halogen bonded complex, an experimental complexation enthalpy in LKr was determined of -15.7(3) kJ mol^{-1}.

When using C_2F_3I as a bond donor molecule, only bands assigned to the halogen bonded complex can be observed. The absence of lp···π complex can be explained by the 22.4 kJ mol^{-1} difference in calculated enthalpy in LXe with the XB complex, resulting in the weaker complex not being able to compete at thermodynamic equilibrium. For the XB complex, a calculated complexation enthalpy of -24.4(2) kJ mol^{-1} was determined in LXe.

From the experimental complexation enthalpies it is clear that the strength of the halogen bond is strongly influenced by the size of the halogen atom involved, with an increase in complexation enthalpy from -8.3(4) kJ mol^{-1} for C_2F_3Cl to -15.7(3) kJ mol^{-1} for C_2F_3Br and -24.4(2) kJ mol^{-1} for C_2F_3I. The influence of the halogen atom on the strength of the lp···π interaction is much smaller, yielding lp···π complexes of similar strength for C_2F_4·TMA(-d_9) and C_2F_3Cl·TMA(-d_9).

Extrapolation of the MP2/aug-cc-pVDZ(-pp) energies to the CCSD(T)/CBS level yields only a limited difference in complexation strength. Comparison of the experimental complexation enthalpies with the calculated enthalpies, determined using the extrapolated complexation energies, shows that the latter values are all higher, but follow the same complexation strength order. It is therefore noteworthy that, even though large basis sets are required in order to obtain accurate energetics for weak intermolecular interactions, the use of smaller basis set also yields correct trends, since these trends are fairly insensitive to the basis set size.[20]

When comparing the experimental results to those of the study involving DME, [26] it is clear that the C(sp²)X XB complexes with TMA still follow the Cl < Br < I bond strength order, but are about 70 % stronger (-9.3(5) vs. -15.7(3) kJ mol^{-1} for Br and -14.2(5) vs. -24.4(2) kJ mol^{-1} for I). For the lp···π bonded complexes, too little data is currently available to reach conclusions concerning bond strength orders. More experimental data involving complexes with other Lewis bases is needed to obtain definitive conclusions concerning the influence of the changing halogen atom on the strength of the lp···π complex.

The experimental confirmation of the existence of the lp···π bonded C_2F_3Cl·TMA(-d_9) complex is also in line with the recent report of Gou et al. [27], in which the C_2F_3Cl·NH_3 lp···π bonded complex was found experimentally using pulsed-jet FTMW. Since the FTMW measurements take place in supersonic expansion, and not at thermodynamic equilibrium, only the complex with the largest complexation energy can be observed, thus disabling the identification of the XB complex with this technique. Indeed, from the results of our calculations shown in Table 2, it can be seen that the lp···π complex has a higher binding energy than the XB complex for C_2F_3Cl·TMA (-19.6 kJ mol^{-1} vs. -15.1 kJ mol^{-1}) at the CCSD(T)/CBS level. However, when applying solvent corrections, this strength order is reversed, leading to a $\Delta H°$ (LKr,calc) of -9.3 kJ mol^{-1} for the lp···π complex and -9.5 kJ mol^{-1} for the XB complex. This comparison also clearly shows that in order to study competing interactions, measurements have to be performed at thermodynamic equilibrium.

Finally, comparison of the experimental complexation enthalpies of the halogen bonded complexes with those of the equivalent CF_3X (Cl, Br, I) complexes shows a slight decrease in bonding strength when the halogen atom is bonded to a sp^2 rather than a sp^3 hybridized carbon atom, which was also observed in the study of C_2F_3X·DME and can be ascribed to the decreased number of electron withdrawing fluorine atoms geminal to the involved halogen atom.

5. Conclusions

Ab initio calculations of the interactions between C_2F_3X (X=F, Cl, Br, I) and TMA yielded lp···π bonded complexes for all four donor molecules, whereas halogen bonded complexes were only found for donor molecules containing Cl or higher halogens. For the halogen bonded complexes, a significant increase in complexation energy, from -15.6 kJ mol^{-1} to -36.5 kJ mol^{-1} at the CCSD(T)/CBS level, is observed going from Cl to I. For the lp···π complexes, complexation energies between -19.6 kJ mol^{-1} and -20.6 kJ mol^{-1} are observed for the complexes with C_2F_3Cl, C_2F_3Br and C_2F_3I, whereas a complexation energy of -16.8 kJ mol^{-1} is found for the complex with C_2F_4. This discrepancy can be attributed to the presence of secondary interactions with the diffuse heavier halogens Cl, Br and I. Experimental assignment of the complexes in the subtracted IR and Raman spectra was aided by harmonic *ab initio* frequency calculations.

Experimentally, lp···π bonded complexes have been observed in noble gas solutions containing C_2F_4 or C_2F_3Cl and TMA(-d_9) at thermodynamic equilibrium using FTIR and Raman spectroscopy, which clearly demonstrates that formation of lp···π interactions is definitely not limited to oxygen based Lewis bases. Moreover, as demonstrated by the simultaneous observation of the C_2F_3Cl·TMA(-d_9) halogen bonded and lp···π complex, these noncovalent interaction are able to coexist. Furthermore, solutions containing C_2F_3Br and TMA(-d_9) in LKr or C_2F_3I and TMA(-d_9) in LXe only yielded halogen bonded complexes.

From temperature studies, complexation enthalpies in LKr were found to be -4.9(1) and -4.9(2) kJ mol^{-1} for the C_2F_4·TMA(-d_9) and C_2F_3Cl·TMA(-d_9) lp···π complex respectively, whereas the C_2F_3Cl·TMA(-d_9) XB complex has a complexation enthalpy of -8.3(4) kJ mol^{-1}. Complexation enthalpies of the halogen bonded complexes of C_2F_3Br and TMA(-d_9) in LKr or C_2F_3I and TMA(-d_9) in LXe have been determined as -15.7(3) kJ mol^{-1} and -24.4(2) kJ mol^{-1} respectively.

The observed complexation strength tendencies are found to be similar to those of the complexes involving dimethyl ether[26] and are in line with the calculated values at the CCSD(T)/CBS level. However, the absolute strength of the halogen bonded complexes involving trimethylamine were found to be stronger than the DME complexes. For the lp···π bonded complexes too little experimental data is currently available to assess whether the difference in strength between the DME and TMA complexes is negligible. From the experiments it is also clear that lp···π interactions are able to compete with weak halogen bonds at thermodynamic equilibrium, which makes them an interesting tool in supramolecular chemistry, crystal engineering and rational drug design. Even though the high directionality of halogen bonds is one of their greatest advantages in these fields of research, it might well be their biggest weakness when competing with other noncovalent interactions, since the high

directionality often does not allow for the formation of additional stabilizing interactions, whereas these are commonly found with hydrogen bonded complexes or lp···π complexes.

Supporting Information Available:

MP2/aug-cc-pVDZ(-PP) cartesian coordinates, vibrational frequencies, IR and Raman intensities of all monomers and complexes, experimental frequencies of C_2F_3X (X= F, Cl, Br) in LKr, C_2F_3I in LXe, TMA and observed complexes, example of the CF_3X·TMA (X = Cl, Br, I) MP2/aug-cc-pVDZ(-PP) equilibrium geometry, NCI plots for all lp···π complexes, IR and Raman spectra of the regions of interest for mixtures involving TMA-d_9 and typical van 't Hoff plots for the XB and lp···π complexes. This material is available free of charge via the Internet at http://pubs.acs.org.

Corresponding Author:

W.A. Herrebout: e-mail: wouter.herrebout@uantwerpen.be, +32/3.265.33.73

Acknowledgements

Y.G. wishes to thank the FWO-Vlaanderen for a doctoral fellowship (11O9514N). W.H. acknowledges financial support through FWO-Vlaanderen and the Special Research Fund BOF (UA). F.D.P. wishes to acknowledge FWO-Vlaanderen and the Free University of Brussels (VUB) for continuous support to the ALGC research group, in particular the VUB for a Strategic Research Program awarded to ALGC, started up at January 1, 2013. The Hercules foundation and the VSC are thanked for generously providing the required CPU resources.

References:

1. Legon, A. C., The Halogen Bond: An Interim Perspective. *Phys. Chem. Chem. Phys.* **2010,** *12*, 7736-7747.
2. Sirimulla, S.; Bailey, J. B.; Vegesna, R.; Narayan, M., Halogen Interactions in Protein-Ligand Complexes: Implications of Halogen Bonding for Rational Drug Design. *J. Chem. Inf. Model.* **2013,** *53*, 2781-2791.
3. Lu, Y. X.; Liu, Y. T.; Xu, Z. J.; Li, H. Y.; Liu, H. L.; Zhu, W. L., Halogen Bonding for Rational Drug Design and New Drug Discovery. *Expert Opin. Drug Discovery* **2012,** *7*, 375-383.
4. Clark, T.; Hennemann, M.; Murray, J. S.; Politzer, P., Halogen Bonding: The σ-Hole. *J. Mol. Model.* **2007,** *13*, 291-296.
5. Donald, K. J.; Wittmaack, B. K.; Crigger, C., Tuning σ-Holes: Charge Redistribution in the Heavy (Group 14) Analogues of Simple and Mixed Halomethanes Can Impose Strong Propensities for Halogen Bonding. *J.Phys. Chem. A* **2010,** *114*, 7213-7222.

6. Tawfik, M.; Donald, K. J., Halogen Bonding: Unifying Perspectives on Organic and Inorganic Cases. *J. Phys. Chem. A* **2014,** *118*, 10090-10100.
7. Metrangolo, P.; Resnati, G.; Pilati, T.; Biella, S., Halogen Bonding in Crystal Engineering. *Struct. Bond.* **2008,** *126*, 105-136.
8. Troff, R. W.; Mäkelä, T.; Topić, F.; Valkonen, A.; Raatikainen, K.; Rissanen, K., Alternative Motifs for Halogen Bonding. *Eur. J. Org. Chem.* **2013,** *2013*, 1617-1637.
9. Murray, J. S.; Lane, P.; Clark, T.; Riley, K. E.; Politzer, P., σ-Holes, π-Holes and Electrostatically-Driven Interactions. *J. Mol. Model.* **2012,** *18*, 541-548.
10. Alkorta, I.; Rozas, I.; Elguero, J., An Attractive Interaction Between the π-Cloud of C_6F_6 and Electron-Donor Atoms. *J. Org. Chem.* **1997,** *62*, 4687-4691.
11. Alkorta, I.; Rozas, I.; Jimeno, M. L.; Elguero, J., A Theoretical and Experimental Study of the Interaction of C_6F_6 with Electron Donors. *J. Struct. Chem.* **2001,** *12*, 459-464.
12. Raimondi, M.; Calderoni, G.; Famulari, A.; Raimondi, L.; Cozzi, F., The Benzene/Water/Hexafluorobenzene Complex: A Computational Study. *J. Phys. Chem. A.* **2003,** *107*, 772-774.
13. Mooibroek, T. J.; Gamez, P.; Reedijk, J., Lone Pair–π Interactions: A New Supramolecular Bond? *CrystEngComm* **2008,** *10*, 1501-1515.
14. Amicangelo, J. C.; Irwin, D. G.; Lee, C. J.; Romano, N. C.; Saxton, N. L., Experimental and Theoretical Characterization of a Lone Pair-π Complex: Water-Hexafluorobenzene. *J. Phys. Chem. A.* **2013,** *117*, 1336-1350.
15. Ma, N.; Zhang, Y.; Ji, B.; Tian, A.; Wang, W., Structural Competition between Halogen Bonds and Lone-Pair···π Interactions in Solution. *ChemPhysChem* **2012,** *13*, 1411-1414.
16. Gung, B. W.; Zou, Y.; Xu, Z. G.; Amicangelo, J. C.; Irwin, D. G.; Ma, S. Q.; Zhou, H. C., Quantitative Study of Interactions Between Oxygen Lone Pair and Aromatic Rings: Substituent Effect and the Importance of Closeness of Contact. *J. Org. Chem.* **2008,** *73*, 689-693.
17. Korenaga, T.; Shoji, T.; Onoue, K.; Sakai, T., Demonstration of the Existence of Intermolecular Lone Pair···π Interaction between Alcoholic Oxygen and the C_6F_5 Group in Organic Solvent. *Chem. Commun.* **2009**, 4678-4680.
18. Egli, M.; Sarkhel, S., Lone Pair-Aromatic Interactions: To Stabilize or not to Stabilize. *Acc. Chem. Res.* **2007,** *40*, 197-205.
19. Danten, Y.; Tassaing, T.; Besnard, M., On the Nature of the Water-Hexafluorobenzene Interaction. *J. Phys. Chem. A.* **1999,** *103*, 3530-3534.
20. Amicangelo, J. C.; Gung, B. W.; Irwin, D. G.; Romano, N. C., Ab Initio Study of Substituent Effects in the Interactions of Dimethyl Ether with Aromatic Rings. *Phys. Chem. Chem. Phys.* **2008,** *10*, 2695-2705.
21. Tsuzuki, S.; Honda, K.; Uchimaru, T.; Mikami, M.; Tanabe, K., Origin of the Attraction and Directionality of the NH/π Interaction: Comparison with OH/π and CH/π Interactions. *J. Am. Chem. Soc.* **2000,** *122*, 11450-11458.
22. Kawahara, S.; Tsuzuki, S.; Uchimaru, T., Lewis Acidity/Basicity of π-Electron Systems: Theoretical Study of a Molecular Interaction Between a π System and a Lewis Acid/Base. *Chem. - Eur. J.* **2005,** *11*, 4458-4464.
23. Yang, T.; An, J. J.; Wang, X.; Wu, D. Y.; Chen, W.; Fossey, J. S., A Theoretical Exploration of Unexpected Amine···π Interactions. *Phys. Chem. Chem. Phys.* **2012,** *14*, 10747-10753.
24. Estarellas, C.; Frontera, A.; Quiñonero, D.; Deyà, P. M., Can Lone Pair-π and Cation-π Interactions Coexist? A Theoretical Study. *Cent. Eur. J. Chem.* **2010,** *9*, 25-34.
25. Berger, G.; Soubhye, J.; van der Lee, A.; Vande Velde, C.; Wintjens, R.; Dubois, P.; Clément, S.; Meyer, F., Interplay between Halogen Bonding and Lone Pair-π Interactions: A Computational and Crystal Packing Study. *ChemPlusChem* **2014,** *79*, 552-558.
26. Geboes, Y.; Nagels, N.; Pinter, B.; De Proft, F.; Herrebout, W. A., On the Competition of C(sp^2)-X···O Halogen Bonding and Lone Pair···π Interactions: A Cryospectroscopic Study of the Complexes of C_2F_3X (X=F, Cl, Br, I) and Dimethyl Ether. *J. Phys. Chem. A* **2015,** *119*, 2502–2516.
27. Gou, Q.; Spada, L.; Geboes, Y.; Herrebout, W. A.; Melandri, S.; Caminati, W., N Lone-Pair···π Interaction: A Rotational Study of Chlorotrifluoroethylene···Ammonia. *Phys. Chem. Chem. Phys.* **2014,** *17*, 7694-7698.

28. van der Veken, B. J., Measurement of Enthalpy Differences in Cryosolutions: Influence of Thermal Expansion. *J. Phys. Chem.* **1996,** *100*, 17436-17438.
29. Frisch, M. J.; Trucks, G. W.; Schlegel, H. B.; Scuseria, G. E.; Robb, M. A.; Cheeseman, J. R.; Scalmani, G.; Barone, V.; Mennucci, B.; Petersson, G. A., et al. *Gaussian 09, Revision D.01*, Gaussian, Inc., Wallingford CT, 2009.
30. Feller, D., The Role of Databases in Support of Computational Chemistry Calculations *J. Comp. Chem.* **1996,** *17*, 1571-1586.
31. Schuchardt, K. L.; Didier, B. T.; Elsethagen, T.; Sun, L.; Gurumoorthi, V.; Chase, J.; Li, J.; Windus, T. L., Basis Set Exchange: A Community Database for Computational Sciences. *J. Chem. Inf. Model.* **2007,** *47*, 1045-1052.
32. Boys, S. F.; Bernardi, F., The Calculation of Small Molecular Interactions by the Differences of Separate Total Energies. Some Procedures with Reduced Errors. *Mol. Phys.* **1970,** *19*, 553-566.
33. Werner, H.-J.; Knowles, P. J.; Knizia, G.; Manby, F. R.; Schütz, M.; Celani, P.; Korona, T.; Lindh, R.; Mitrushenkov, A.; Rauhut, G., et al. *MOLPRO, version 2012.1, A Package of Ab Initio Programs*, 2012.
34. Truhlar, D. G., Basis-Set Extrapolation. *Chem. Phys. Lett.* **1998,** *294*, 45-48.
35. Jurecka, P.; Hobza, P., True Stabilization Energies for the Optimal Planar Hydrogen-Bonded and Stacked Structures of Guanine···Cytosine, Adenine···Thymine, and Their 9-and 1-Methyl Derivatives: Complete Basis Set Calculations at the MP2 and CCSD(T) Levels and Comparison with Experiment. *J. Am. Chem. Soc.* **2003,** *125*, 15608-15613.
36. Jorgensen, W. L., *BOSS - Biochemical and Organic Simulation System*. John Wiley & Sons Ltd., New York, 1998.
37. Hauchecorne, D.; van der Veken, B. J.; Moiana, A.; Herrebout, W. A., The C–Cl···N Halogen Bond, the Weaker Relative of the C–I and C–Br···N Halogen Bonds, Finally Characterized in Solution. *Chem. Phys.* **2010,** *374*, 30-36.
38. Johnson, E. R.; Keinan, S.; Mori-Sanchez, P.; Contreras-Garcia, J.; Cohen, A. J.; Yang, W. T., Revealing Noncovalent Interactions. *J. Am. Chem. Soc.* **2010,** *132*, 6498-6506.
39. Contreras-Garcia, J.; Johnson, E. R.; Keinan, S.; Chaudret, R.; Piquemal, J. P.; Beratan, D. N.; Yang, W., NCIPLOT: A Program for Plotting Non-Covalent Interaction Regions. *J. Chem. Theory Comput.* **2011,** *7*, 625-632.
40. Herzberg, G., *Infrared and Raman Spectra of Polyatomic Molecules*. 12th ed.; D. Van Nostrand Company Inc., Princeton, New Jersey, 1945.
41. Singh, S. K.; Das, A., The n→π* Interaction: A Rapidly Emerging Non-Covalent Interaction. *Phys. Chem. Chem. Phys.* **2015,** *17*, 9596-9612.
42. Herrebout, W. A., Infrared and Raman Measurements of Halogen Bonding in Cryogenic Solutions. *Top. Curr. Chem.* **2015,** *358*, 79-154.

Graphical abstract for Table of contents: